Meshfree Analysis Using the Generalized Meshfree (GMF) Approximation

Chung-Kyu Park*, Cheng-Tang Wu** and Cing-Dao (Steve) Kan*
*National Crash Analysis Center (NCAC), The George Washington University, Ashburn, VA
**Livermore Software Technology Corporation (LSTC), Livermore, CA

Abstract

Meshfree methods are becoming widely used in many industrial fields since the finite element method (FEM) has inherent limitations, such as mesh quality and related distortion problems, to analyze sophisticated problems under large deformation. However, the meshfree methods also have their own deficiencies, mainly the high CPU cost.

Recently, the generalized mesh-free (GMF) approximation is developed to improve the efficiency and accuracy in the conventional meshfree methods for solid analysis. The GMF approximation is the integrated formulation to generate existing approximations, such as moving least square (MLS), reproducing kernel (RK), and maximum entropy (ME) approximation, as well as new approximations based on the selection of a basis function. The GMF approximation has two excellent features. The one is that the GMF approximation naturally bears the weak Kronecker-delta property at boundaries, which makes the imposition of essential boundary conditions in meshfree methods easier. The other is that the GMF approximation can be extended to higher-order approximations, which can improve the accuracy of meshfree methods.

In this study, some meshfree analyses are performed by LS-DYNA® to demonstrate the performance and accuracy of the GMF approximation. The results show that the convex approximation gives better performance and accuracy than the non-convex approximation in meshfree analysis.

Introduction

Today, computer-aided engineering (CAE) analysis has become a very powerful and indispensable tool in almost all engineering fields. In automotive industry, engineers and designers rely heavily on CAE analysis for vehicle component designs, structural optimizations, and vehicle crashworthiness evaluations. For example, the finite element method (FEM) based CAE tool is routinely used for vehicle crashworthiness and enables the engineers to assess vehicle structural and occupant safety under many different impact scenarios in a robust and accurate way.

Thanks to the rapid improvement of computers, engineers attempt to apply the FEM-based CAE analysis to solve very sophisticated problems with high-accuracy expectation. However, the FEM has inherent limitations to satisfy their expectation. One of the well-known limitations in the FEM comes from the mesh quality and related mesh distortion problems. Examples are severe mesh distortion of honeycomb barriers in vehicle crash simulations, rubber materials of crash test dummies in occupant safety analyses, soil and wood materials in road-side safety analyses, and brittle vehicles components in car-to-car crash simulations. As a result, the FEM suffers from numerical instability, and may yield non-physical results due to the distortion of the mesh.

In the mid 1990's, the meshfree methods, such as the element-free Galerkin (EFG) method [1] and the reproducing kernel particle method (RKPM) [2], were proposed as a solution to improve the mesh quality problems involving in the FEM. The meshfree methods have been applied to many problems with success. Wang *et al*. utilized the meshfree methods for the development of honeycomb barriers and a rubber material within crash test dummies in automotive crashworthiness simulations [3]. However, the meshfree methods have their own deficiencies, mainly the high CPU cost.

In the meshfree methods, the approximations based on the moving least square (MLS) method [1,4] or the reproducing kernel (RK) method [2] are non-convex approximations. Unfortunately, those non-convex approximations do not bear the Kronecker-delta property at the boundaries which is an important and convenient property to enforce the essential boundary conditions. Therefore, special boundary condition treatments are required for the meshfree methods, which increases the computation time considerably and sometimes even degrades the accuracy. The maximum entropy (ME) approximation [5,6] is a convex meshfree approximation and bears the weak Kronecker-delta property at boundaries.

Recently, the new approach for the construction of meshfree approximation, the so-called generalized meshfree (GMF) approximation, is developed [7,8]. The GMF approximation is the general approximation to produce existing approximations as well as new approximations with possessing the weak Kronecker-delta property at the boundaries regardless of whether convex or non-convex, which makes the essential boundary conditions impose straightforward and reduces the computational time in the meshfree methods. In this study, some meshfree analyses are conducted to account for the performance and accuracy of the GMF approximation.

Generalized Meshfree (GMF) Approximation [7,8]

The first-order GMF approximation in one dimension is described as follows:

$$\Psi_i(\mathrm{x},\lambda)=\frac{\psi_i}{\psi}=\frac{\phi_a(\mathrm{x};X_i)\Gamma_i(X_i,\lambda)}{\sum_{j=1}^{n}\phi_a(\mathrm{x};X_j)\Gamma_j(X_j,\lambda)} \quad \text{for fixed } \mathrm{x}, \tag{1}$$

subjected to

$$R(\mathrm{x})=\sum_{i=1}^{n}\Psi_i X_i=0 \quad \text{(linear constraints)}, \tag{2}$$

where $\psi_i=\phi_a(\mathrm{x};X_i)\Gamma_i(X_i,\lambda)$, (3)

$$\psi=\sum_{i=1}^{n}\psi_i=\sum_{i=1}^{n}\phi_a(\mathrm{x};X_i)\Gamma_i(X_i,\lambda), \tag{4}$$

$$X_i=\mathrm{x}-\mathrm{x}_i, \tag{5}$$

x is the coordinate of interior point (fixed point),

x_i is the coordinate of node i,

$\phi_a(\mathrm{x};X_i)$ is the weighting function of node i with support size $a(\mathrm{x})$,

$\Gamma_i(X_i,\lambda)$ is the basis function,
n is the number of nodes within the support size $a(\mathrm{x})$ at fixed x, and
$\lambda(\mathrm{x})$ is the constraint parameter which has to be decided.

The spatial derivative of the GMF approximation is given by

$$\frac{d\Psi_i}{dx} = \Psi_{i,\mathrm{x}} + \Psi_{i,\lambda}\lambda_{,\mathrm{x}} \tag{6}$$

where $$\Psi_{i,\mathrm{x}} = \frac{\psi_{i,\mathrm{x}}}{\psi} - \Psi_i \sum_{j=1}^{n} \frac{\psi_{j,\mathrm{x}}}{\psi}, \tag{7}$$

$$\psi_{i,\mathrm{x}} = \phi_{a,\mathrm{x}}\Gamma_i + \phi_a \Gamma_{i,\mathrm{x}}, \tag{8}$$

$$\Psi_{i,\lambda} = \frac{\phi_a \Gamma_{i,\lambda}}{\psi} - \Psi_i \sum_{j=1}^{n} \frac{\phi_a \Gamma_{j,\lambda}}{\psi}, \tag{9}$$

$$\lambda_{,\mathrm{x}} = -J^{-1} R_{,\mathrm{x}}, \tag{10}$$

$$J = \sum_{i=1}^{n} \frac{\phi_a \Gamma_{i,\lambda}}{\psi} X_i - R \sum_{j=1}^{n} \frac{\phi_a \Gamma_{j,\lambda}}{\psi}, \tag{11}$$

$$R_{,\mathrm{x}} = \sum_{i=1}^{n} \Psi_{i,\mathrm{x}} X_i + 1. \tag{12}$$

In the GMF approximation, the property of the partition of unity is automatically satisfied by the normalization in Eq. (1). Basically, any kind of function can be used as a basis function in the GMF approximation if the function is monotonically increasing or decreasing. By choosing appropriate basis functions, some well-known convex or non-convex approximations, such as Shephard, ME, MLS, and RK approximations, can be recovered. The completion of the GMF approximation is achieved by finding λ to satisfy Eq. (2). To determine λ at any fixed x in Eq. (1), a root-finding algorithm is required for the non-linear basis functions.

One of the special properties of the convex approximation is the satisfaction of the weak Kronecker-delta property at the boundaries, while the non-convex approximation doesn't bear this property. The weak Kronecker-delta property at the boundaries in the convex approximation is naturally coming from satisfying the convexity of the approximation. In order to impose the weak Kronecker-delta property at the boundaries in the non-convex approximation, the boundary correction function, Eq. (13), is defined to achieve local convexity at boundary nodes as shown below

$$C_B(X_j,\lambda,D_j) = \prod_{j=n_1}^{n_{EB}} e^{\lambda X_j D_j} \tag{13}$$

where $$\prod_{j=n_1}^{n_{EB}} e^{\lambda X_j D_j} = e^{\lambda X_{n_1} D_{n_1}} \times e^{\lambda X_{n_2} D_{n_2}} \times \cdots \times e^{\lambda X_{n_{EB}} D_{n_{EB}}}, \tag{14}$$

$D_j = \phi_{r_j^{EB}}(\mathrm{x}; X_j)\cdot P_j$ is the kernel function at essential boundary nodes, (15)

r_j^{EB} is the support size of the kernel function at essential boundary nodes,

P_j is the penalty constant.

The boundary correction function, Eq. (13), becomes unity outside the boundary supports and it takes the exponential form within the support of boundary nodes. Then, the shape function of Eq. (3) is rewritten as

$$\psi_i = \phi_a(\mathrm{x}; X_i)\Gamma_i(X_i, \lambda)C_B(X_j, \lambda, D_j) = \phi_a(\mathrm{x}; X_i)\tilde{\Gamma}_i(X_i, \lambda, D_j), \tag{16}$$

$$\tilde{\Gamma}_i(X_i, \lambda, D_j) = \begin{cases} 1+(\lambda X_i) & , \text{ out of boundary support} \\ [1+(\lambda X_i)]e^{\lambda X_{n_j} D_{n_j}} & , \text{ inside boundary support of } N_j \end{cases}. \tag{17}$$

$\tilde{\Gamma}_i(X_i, \lambda, D_j)$ can be considered as a modified or corrected basis function corresponding to essential boundary nodes. The penalty constant plays a role in making the decay of exponential function faster and simplifying root-finding of λ to meet the linear constraint within a support size r_j^{EB}. In this approach, the weak Kronecker-delta property at the boundaries is imposed in constructing the non-convex approximation, and the approach is independent of solving discretized partial differential equation (PDE).

Figure 1(a) compares the shape functions of MLS and the shape functions of GMF with exponential basis function, GMF(*exp*), with a non-uniform discretization shown in Figure 2. Figure 1(b) demonstrates that the Kronecker-delta property at the boundaries is achieved by the proposed method while the rest of shape functions away from the boundary remains the same as the original MLS approximation, which is named as the GMF(*MLS*) approximation. That is to say, the GMF(*MLS*) approximation is the non-convex MLS approximation with weak Kronecker-delta property at the boundaries. The other special feature of the GMF approximation is to extend to higher order approximation, which is described in the references [7,8].

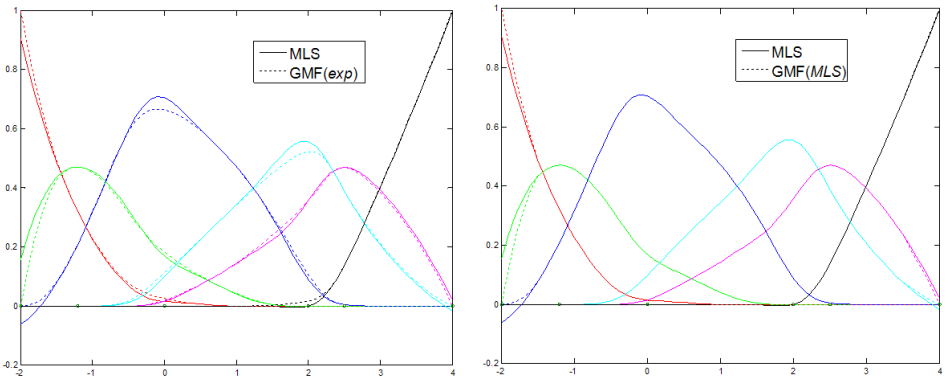

(a) (b)

Figure 1. Shapes of MLS and GMF approximations.

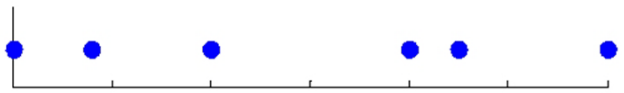

Figure 2. Description of non-uniform discretization models in 1D

Applications of GMF Approximation

Some features of the GMF approximation are already implemented in the LS-DYNA code and ready to use. In this study, we performed some meshfree analyses to demonstrate the performance and accuracy of the GMF approximation. In the analyses, the GMF(*MLS*), GMF(*exp*) and GMF(*atan*) approximations are utilized in the meshfree framework. The GMF(*MLS*) approximation, which is the non-convex approximation, is the MLS approximation with local convexity to impose essential boundary conditions. The GMF(*exp*) and GMF(*atan*) approximations are the convex approximations with exponential and arc-tangent basis functions respectively.

Cantilever beam

In this example, a 3D cantilever beam as shown in Figure 3 is analyzed to study the convergence of the GMF approximations with different basis functions. The beam is fixed at one end and is subjected to a parabolic traction (*P*) at the other end. The analytical solution is obtained by assuming that the Poisson's ratio is zero and a plane stress condition is considered [9]. The analytic solution is given as

$$u_x = -\frac{Py}{6EI}\left[(6L-3x)x+(2+\nu)\left(y^2-\frac{D^2}{4}\right)\right], \text{ and} \tag{18}$$

$$u_y = \frac{P}{6EI}\left[3\nu y^2(L-x)+(4+5\nu)\frac{D^2x}{4}+(3L-x)x^2\right] \tag{19}$$

where the moment of the inertia of the beam is $I = D^3/12$. The following parameters are used for this problem: Young's modulus E = 1000, L = 50, D = 10, and B = 1. Both uniform and non-uniform discretizations shown in Figure 4 are used for the analysis using $3\times3\times3$ Gaussian quadrature with normalized support size $a = 1.5$ in the meshfree computation. The FEM analysis is also performed using a fully integrated linear element for the comparison.

The results of L_2 norm error in displacement are shown in Figure 5(a) and (b) for the uniform and non-uniform discretizations respectively. The GMF approximations with three different basis functions present similar accuracy in both uniform and non-uniform discretizations. Further, the accuracy and convergence of the meshfree method are better than the FEM in this study. The displacement distributions along the mid-surface shown in Figure 6(a) and (b) further confirm the accuracy of the meshfree method. Note that the support size in the non-uniform discretizations is slightly larger than that of the uniform discretizations. This is the reason that the non-uniform model predicts a slightly better tip displacement solution than the uniform model when normalized support $a = 1.5$ is adopted in the analysis.

Next, the effects of support size and integration order are investigated for employing the three basis functions in the GMF approximation. When a normalized support size less than two is used in the analysis, three basis functions give similar tip displacement results for both discretizations as shown in the plots from Figure 7(a) and (b) to Figure 9(a) and (b). On the other hand, significant errors in the GMF(*MLS*) approximation are observed when the normalized support is greater than 2.0 regardless of the integration order. This is probably due to the non-convexity in

the GMF(*MLS*) approximation. It is also observed that the GMF(*exp*) approximation presents the best displacement solution among the three basis functions. The difference between the GMF(*exp*) and the GMF(*atan*) approximations is marginal when the normalized support is less than 2.5. However, a stiff response is observed in the GMF(*atan*) approximation when a larger support size is used. The results suggest that the convex approximation exhibits better accuracy and convergence than the non-convex approximation especially when the support size is large.

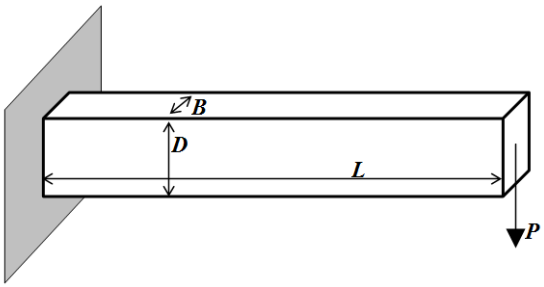

Figure 3. 3D cantilever beam

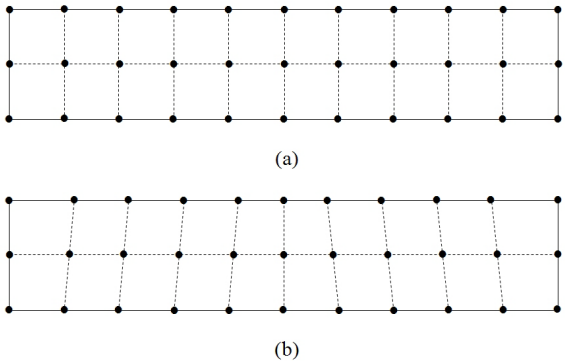

Figure 4. Discretization of cantilever beam: (a) Regular model; (b) Irregular model

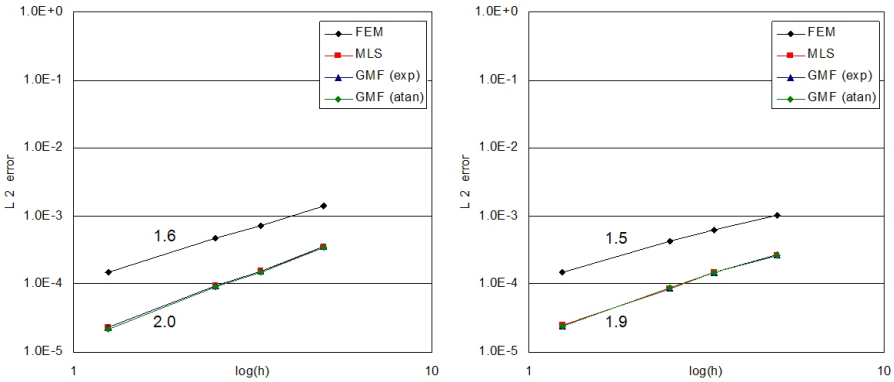

Figure 5. L_2 error: (a) Regular model; (b) Irregular model

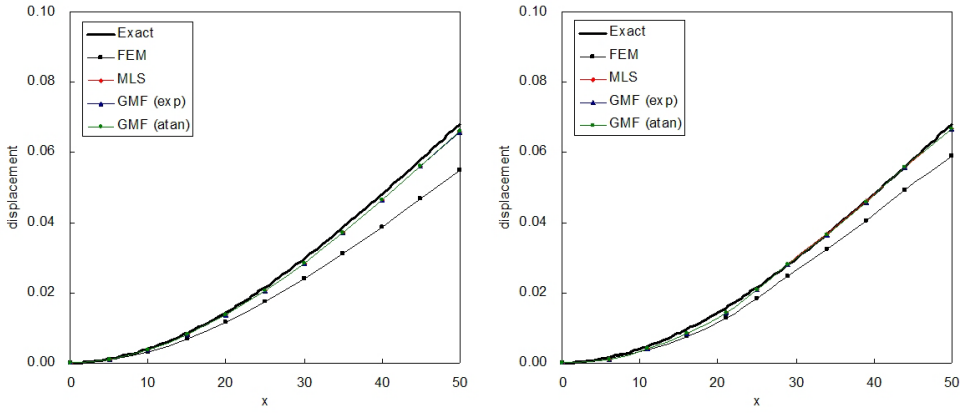

Figure 6. Displacement profiles of a cantilever beam: (a) Regular model; (b) Irregular model

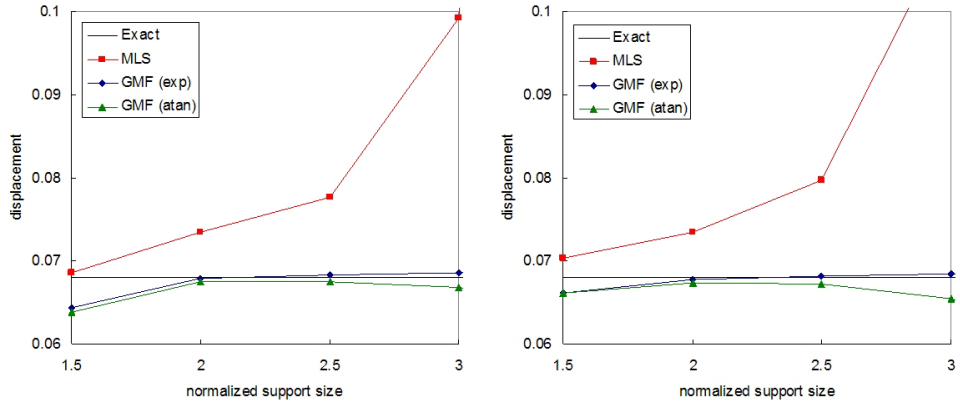

(a) (b)

Figure 7. Tip displacement of a cantilever beam ($2\times2\times2$ Gaussian quadrature): (a) Regular model; (b) Irregular model

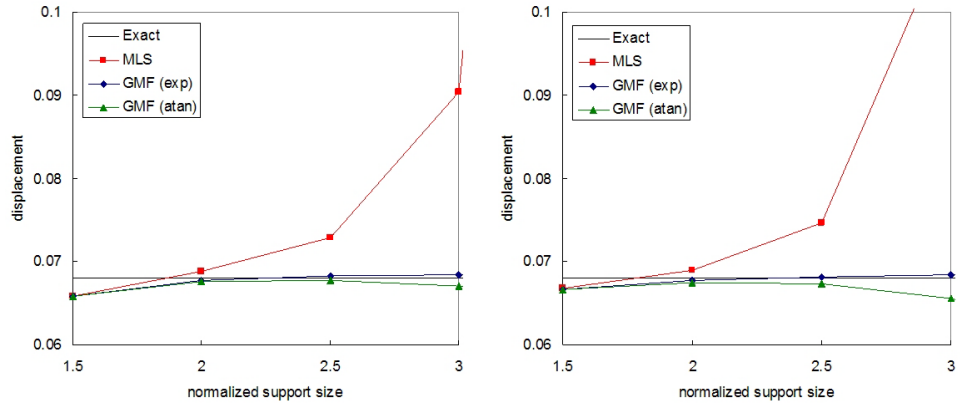

(a) (b)

Figure 8. Tip displacement of a cantilever beam ($3\times3\times3$ Gaussian quadrature): (a) Regular model; (b) Irregular model

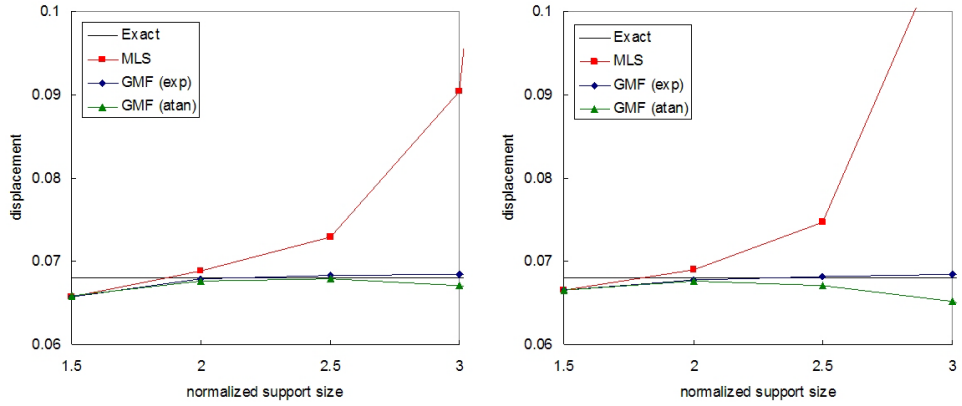

(a) (b)

Figure 9. Tip displacement of a cantilever beam ($4\times4\times4$ Gaussian quadrature): (a) Regular model; (b) Irregular model

Compression of a ring

This problem is analyzed to examine the effectiveness of three GMF approximations for the nonlinear analysis as well as for elastic contact. A ring compressed by two rigid plates with frictionless contact condition is shown in Figure 10. The bottom rigid plate is fixed and the top rigid plate is moved downward by a force control $F = 2.1 \times E5$ in 14 incremental steps. Two types of materials are considered in the analysis including the elastic material and rubber-like material. The material constants are gives as follows: Young's modulus E = 1000, Poission's ratio is chosen to be 0.3 for elastic ring and is 0.49 for the rubber ring. A normalized support size of 1.5 with 3×3×3 integration order is used in the meshfree analysis. A FEM solution using fully integrated linear element with very fine mesh is considered as a reference solution.

Figure 11(a) shows the load-displacement curves for the case of ν = 0.3. Since volumetric locking is not an issue, all three meshfree methods generate good solutions. The FEM solution displays a slightly stiff result compared to the meshfree solution when same discretization model (coarse mesh) is used. Superior performance of the meshfree method over FEM is presented in the load-displacement curves for the case of ν = 0.49 as shown in Figure 11(b). All three meshfree methods generate good solutions. In contrast, FEM with fully integrated linear element displays a poor performance in nearly-compressible case when a coarse model is used.

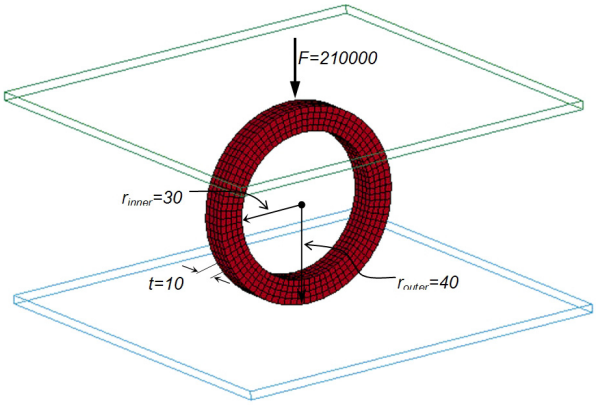

Figure 10. Ring compression model.

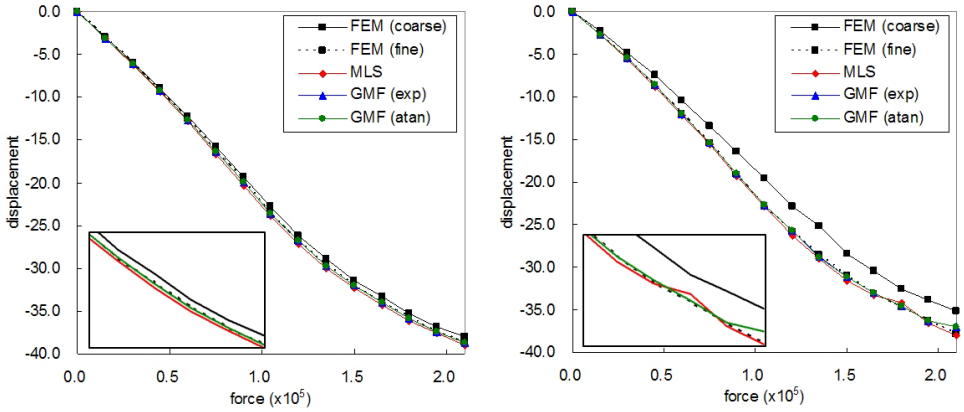

(a) (b)

Figure 11. Comparison of load-displacement curves (inside plots magnify the end part of the curves): (a) The case of ν = 0.3; (b) The case of ν = 0.49.

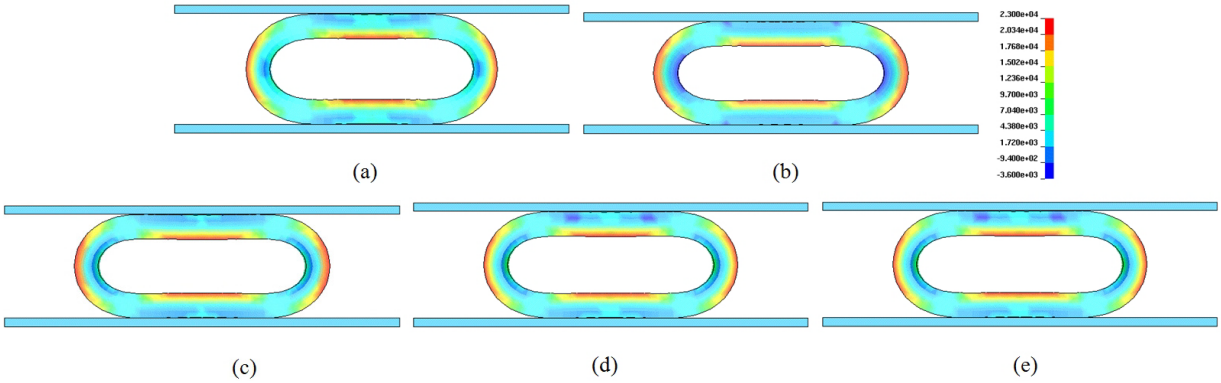

Figure 12. Final deformation in maximum principle stress: (a) FEM (coarse); (b) FEM (fine); (c) MLS; (d) GMF(*exp*); (e) GMF(*atan*).

Compared with solutions obtained by the meshfree convex approximations, the oscillation is observed in the MLS approximation as shown in Figure 11(b). Similarly, oscillation is also observed in the FEM solution with coarse mesh. The final deformation of three meshfree methods also match quite well with that of the FEM with very fine mesh as shown in Figure 12(b)-(e) where the FEM deformation with coarse mesh predicts a stiff result.

Compression of foam

The following example is used to identify the applicability of the GMF approximations to a large deformation analysis of a highly non-linear foam material. The highly compressible foam is commonly used in many automotive crashworthiness simulations. The FEM analysis sometimes suffers from numerical difficulties in modeling large material distortion.

A 3D compression simulation of low-density foam material is performed. The simulation model is shown in Figure 13(a). In this analysis, the bottom of the foam is fixed, and the rigid punch is moved downward with a prescribed velocity of 3.33 *mm/s*. The low-density foam material is modeled by the material type 57 (*MAT_LOW_DENSITY_FOAM) in the material database of LS-DYNA [10,11]. The parameters of this foam material model are taken as; density (ρ) is $24\,kg/m^3$, Young's modulus (E) is 0.25 *MPa*, and the nominal stress versus strain characteristic of the foam is plotted in Figure 13(b). The dimension of the foam is $100mm\times100mm\times100mm$ and the area of punch is $40mm\times40mm$. The foam is modeled with $21\times21\times21$ nodes with $20\times20\times20$ integration zones. The explicit time integration method with lumped mass is employed. For a fair comparison of CPU times using different approximation methods including FEM, a $2\times2\times2$ integration order is adopted in the analysis. A normalized support size of 1.5 is used in the meshfree analysis.

Figure 14 compares the force history curves measured at the punch with four different methods. The mixed-transformation method [12] is used to treat the boundary conditions in the MLS approximation, which is named as MLS(m-trans). Each symbol in the plot indicates the termination time of each punch test. The results indicate that their responses are fairly overlapped but the meshfree methods allow larger deformation than FEM. Figure 15 shows the final deformed shapes of the foam along the symmetric plane. The compression ratio in Figure 15 is defined as

$$\text{Compression ratio (\%)} = \frac{\text{Maximum compressed displacement by punch}}{\text{Initial height of foam}} \times 100 \,. \qquad (20)$$

The results show that the convex approximation behaves more robust than non-convex approximation in handling large material distortion. The GMF(*atan*) approximation behaves the best among three basis functions since it allows the largest deformation comparing to the others. A comparison of normalized CPU time using different methods is listed in Table 1. The final punching depth in FEM is used as a reference for the comparison. All the three meshfree methods are re-analyzed to obtain the corresponding CPU time based on the same punching depth. Noted that MLS(m-trans) requires a slightly higher CPU time compared to the GMF(*exp*) and the GMF(*atan*) approximations. The extra effort in the boundary condition treatment in the MLS approximation is now avoided in GMF(*exp*) and the GMF(*atan*) approximations.

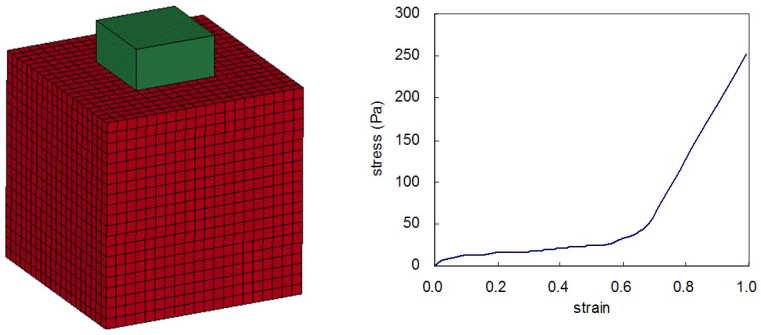

Figure 13. Description of a model and foam material property: (a) Setup of a compression test; (b) Strain vs. stress curve of foam material.

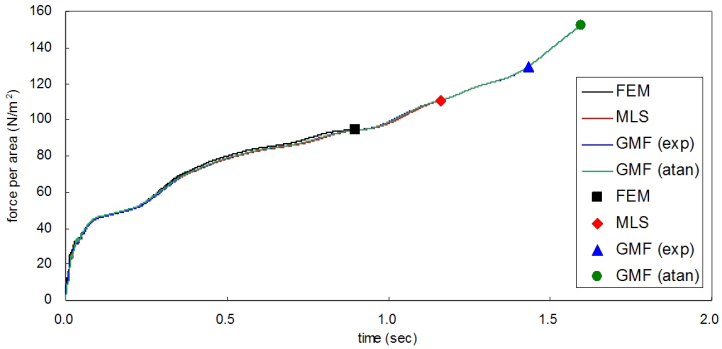

Figure 14. Force history (each symbol indicates the termination time of each punch test)

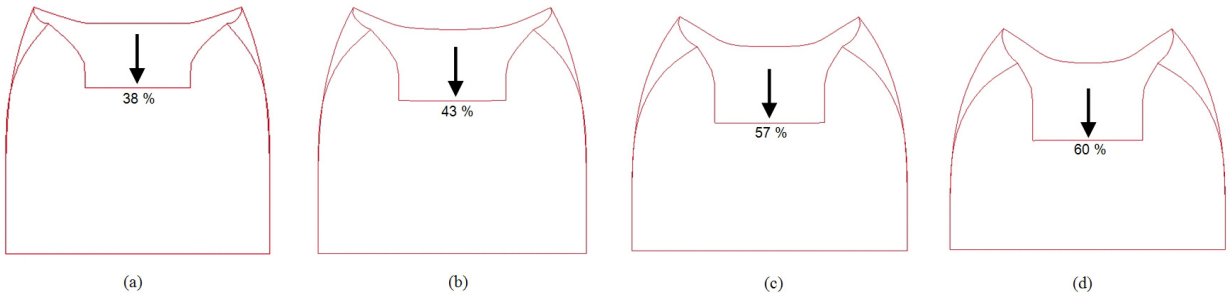

Figure 15. Maximum deformed shapes of the mid section of form: (a) FEM; (b) MLS; (c) GMF (exp); (d) GMF (atan).

Table 1. CPU time comparison of foam compression.

	FEM	MLS(m-trans)	GMF(*exp*)	GMF(*atan*)
Normalized CPU time	1.0	3.1	2.8	2.8

Summary

The GMF approximation is the integrated formulation to generate existing approximations, such as MLS, RK, and ME approximations, as well as new approximations based on the selection of a basis function. The completion of the GMF approximation is achieved by finding constraint parameters which satisfy constraint equations. The GMF approximation has two excellent features. The one is that the GMF approximation naturally bears the weak Kronecker-delta property at boundaries, which makes the imposition of essential boundary conditions in meshfree methods easier. The other is that the GMF approximation can be extended to higher-order approximations, which can improve the accuracy of meshfree methods

Three meshfree analyses are conducted by LS-DYNA to describe the performance and accuracy of the GMF approximation. The results show that the convex approximations, the GMF(*exp*) and GMF(*atan*) approximations, give better accuracy and performance than the non-convex approximation, the MLS approximation. Especially, the GMF(*atan*) approximation shows good robustness in large deformation.

References

1. Belytschko T, Lu YY, Gu L, "Element-free Galerkin methods", *International Journal for Numerical Methods in Engineering* 1994, 37(2) pp. 229-256.
2. Liu WK, Jun S, Zhang YF, "Reproducing kernel particle methods", *International Journal for Numerical Methods in Fluids* 1995, 20 pp. 1081-1106.
3. Wang HP, Wu CT, Guo Y, Botkin ME, "A coupled meshfree/finite element method for automotive crashworthiness simulations", *International Journal of Impact Engineering* 2009, 36 pp. 1210-1222.
4. Lancaster P, Salkauskas K, "Surfaces generated by moving least squares methods", *Mathematics of Computation* 1981, 37 pp. 141-158.
5. Arroyo M, Ortiz M, "Local maximum-entropy approximation schemes: a seamless bridge between finite elements and meshfree methods", *International Journal for Numerical Methods in Engineering* 2006, 65 pp. 2167-2202.
6. Sukumar N, "Construction of polygonal interpolants: a maximum entropy approach", *International Journal for Numerical Methods in Engineering* 2004, 61 pp. 2159-2181.
7. Wu CT, Park CK, Chen JS, "A generalized approximation for the meshfree analysis of solids", *International Journal for Numerical Methods in Engineering* 2010, Submitted.
8. Park CK, *The development of a generalized meshfree approximation for solid and fracture analysis*, Dissertation, 2009, The George Washington University, DC, USA.
9. Timoshenko SP, Goodier JN, *Theory of Elasticity*, 1970, McGraw-Hill, NY, USA.
10. Hallquist J.O., *LS-DYNA® Theory Manual*, 2006, LSTC, CA, USA.
11. LSTC, *LS-DYNA®Kkeyword User's Manual*, Version 971, 2007, LSTC, CA, USA.
12. Chen JS, Wang HP, "New boundary condition treatments in meshfree computation of contact problems", *Computer Methods in Applied Mechanics and Engineering* 2000, 187 pp. 441-468.